RSC Advances

ROYAL SOCIETY OF CHEMISTRY

www.rsc.org/advances

Size-control synthesis, characterization and electrocatalytic behaviors of polymer-protected nickel nanoparticles: A comparison with respect to two polymers

Partha Sarathi Roy and Swapan Kumar Bhattacharya*

Physical Chemistry Section, Department of Chemistry,

Jadavpur University, Kolkata – 700 032, India.

***Email – skbhatt7@yahoo.co.in,**

Tel.: +919831699643, Fax: +913324146584

Abstract

A facile reduction approach of nickel chloride in aqueous solution with sodium borohydride leads to fairly monodisperse, and electrochemically active nickel nanoparticles by the separate use of capping polymer like polyvinyl pyrrolidone (PVP) and polyacrylic acid (PAA). The resulting nanoparticles have been characterized by transmission electron microscopy, powder X-ray diffraction, Fourier transform infrared spectroscopy, and cyclic voltammetry. The size of the Ni nanoparticles is very small (1.2-6.1 nm) and can be readily tuned by changing the polymer as well as its concentration in each case. PVP bearing bulky pyrrolidone moiety leads to the formation of smaller nanoparticles than PAA at the chosen concentrations of polymers providing almost similar number of monomer units. In alkaline medium graphite-supported Ni nanoparticles form $Ni(OH)_2$ and then NiOOH which are electrocatalytically active towards the electro-oxidation of methanol. The study reveals that at high positive potential polyacrylate anion interacts more with the catalyst nanoparticles as compared to PVP resulting lowering of current density at higher concentration of polymer. Thus the catalyst nanoparticles are capable to exhibit competing effects of size- and particle-

surface-environment in electrocatalysis and possess alcohol sensing property for alkaline oxidation of methanol.

Keywords

Size-control synthesis; Nickel nanoparticles; Electrocatalysis; Competing effects in catalysis;

Introduction

Nanomaterials have been explored extensively for the fundamental scientific and technological interests in accessing new classes of functional materials with unprecedented properties and applications.[1–6] In the recent years, nickel nanoparticles have become one of the interesting metallic nanomaterials in research communities due to diverse promising applications in the field of chemical catalysis, electrocatalysis, conducting paints, magnetic recording, rechargeable batteries, medical diagnosis, superconducting device, and so on.[1, 6] Nickel particles were reported to be excellent catalysts for hydrogenation of nitrobenzene and nitrophenol, oxygen reduction, and oxidation of olefins.[7] Besides this, cheaper nickel nanoparticles are also used as a component of the modified electrodes for alcohol sensing[8] and fuel cell development[9] particularly in alkaline medium although electrocatalytic activity of bare Ni foil is insignificant at low potential.[10] Thus considering urgent demand, much recent research has still been focused on improving the factors that control the shape, size and properties of Ni nanoparticles.

Among all the magnetic metallic nanomaterials, nickel nanostructured materials are comparatively difficult to prepare as they are easily oxidized.[11] Over the last decades, various chemical and physical approaches have been developed in order to overcome this difficulty and to prepare high-quality nickel nanoparticles. Polyol process[4], chemical reduction in the liquid phase[11], ball milling[12], electrodeposition[13], decomposition of organometallic precursors[14], chemical vapor deposition (CVD)[15], thermal plasma[16], modified electroless plating[17], laser ablation[18], large-scale spray pyrolysis[19], microwave-assisted synthesis[20] and many other methods[11] have been applied to obtain varieties of metallic nickel nanoparticles.

However, among the various synthetic approaches developed, the solution phase chemistry routes can satisfactorily provide facile and diverse ways to achieve the control over particle size, morphology, crystalline phase and other properties. On the other hand, among the

various solution phase chemistry routes, the reduction of metal salts is the most common, and reducing agents such as $NaBH_4$[21, 22], hydrazine[23–26], alkylamines[6], and polyols[27–29] have been commonly employed in the reactions. It is also noteworthy that according to the desired properties of the resultant nanocrystals, the manipulation and economical aspects of the process, chemical reduction of cations from the solution of metal salts using strong reducing agents may be the best way to prepare nickel nanomaterials. Ni nanoparticles synthesis by $NaBH_4$ reduction is chosen because it is a method of obtaining small nanoparticles in aqueous medium by a fast, cost effective synthetic route at room temperature.

However in chemical methods, polymers have been commonly used to prevent the nanoparticles from coalescing and sterically protect the particles. In particular, polymers can stabilize metal nanoparticles through the steric bulk of their framework and also by binding weakly to the nanoparticle surface through heteroatoms that act as ligands.[3] In this regard water soluble capping polymers (steric stabilizer) e.g., polyvinylpyrrolidone (PVP), polyacrylic acid (PAA) etc. have been often used.[30–33] It has been also reported that polymers are able to control shape and size of the nanoparticles[34]. Again, polymer-stabilized metal nanoparticles can be uniformly dispersed in organic solvents or water and mixed with reactants and products in a way resembling a homogeneous catalytic system.[35] Previously we have used polyvinyl alcohol (PVA), a water soluble polymer to synthesize electro-catalytically active palladium[36-38] and platinum[39] nanoparticles. Notably, in practice PVA fails to synthesize stable Ni nanoparticles because of the fact that liophilic PVA coagulates and separates from aqueous colloidal solution under the action of $NaBH_4$. Herein we have prepared electrochemically active nickel nanoparticles using two polymers, PVP and PAA, separately and compared their characteristics including electrocatalytic activity with respect to electro-oxidation of alkaline methanol. As a medium of synthesis or catalytic environment two polymers of different concentration are not amenable to comparison. So, three pairs of

solutions of two polymers, having similar concentrations are produced for synthesis and characterization of Ni nanoparticles. It is well known that small nanoparticles are better catalysts because of large surface-to-volume ratio and involvement of high energized molecules at the surface in catalysis. Again smaller nanoparticles are usually synthesized in medium containing greater amount of capping polymer, the presence of which reduces the catalytic activity. So it would be of interest to note which of the two factors dominate to control the catalytic activity of the nanoparticles. Here the particle size has been decreased by increasing the concentration of the polymer and the compound effect on changing the catalytic activity is followed. The aim of this work is to study the effect of the polymer on the particle-size and catalytic activity of nano-nickel, in the environment of same and different concentrations of monomer units of two polymers having different and same functional groups.

Experimental

Materials

Polyvinylpyrrolidone (PVP, K-30, relative molar mass $(111.15)_x$) was the product of S.D. fine chem. Ltd. and polyacrylic acid (PAA, approx. relative molar mass = 2,000; 63 wt% solution in water, density = 1.230 gcm^{-3}) was from Across organics, New Jersey, USA. Nickel(II) chloride hexahydrate ($NiCl_2$, $6H_2O$) and sodium borohydride ($NaBH_4$) were purchased from Merck, India. Other reagents were at least AR/GR grade and used without further purification. Water used through out this work was reagent grade, produced by a Milli–Q Ultra-Pure-Water purification system of Millipore.

Synthesis of polymer protected nickel nanoparticles

A typical example for the preparation of PVP-stabilized nickel nanoparticles (sample A) is described as follows. PVP (~ 0.30 g, 2.70 mmol in terms of monomeric units) was dissolved in about 36 ml of water by gentle stirring. $NiCl_2$, $6H_2O$ (6 ml of 2%, 0.50 mmol)

was added to the mixture and mixed well. This was followed by addition of solid $NaBH_4$ (0.2 g, 5.29 mmol) in a single act under well stirring condition of the mixture. Within one minute of the addition of $NaBH_4$, 2 mmol of NaOH was added and immediately volume of the solution was made up to 50 ml by water. Other samples B and C were prepared in the similar way as sample A by changing the concentrations of PVP. For samples B and C, the amounts of PVP taken were ~1.2 and 4.8 g, corresponding to 10.80 and 43.18 mmol of PVP (in terms of monomeric units), respectively. After the addition of NaOH and water all the samples reached the pH ranging from 11 to 12.

Similarly, for the other set, a typical example for the preparation of PAA-protected nickel nanoparticles (sample D) is as follows. PAA (~ 0.4 g of 63 wt% solution, 2.89 mmol in terms of monomeric units) was dissolved in about 18 ml of water by gentle stirring. $NiCl_2$, $6H_2O$ (6 ml of 2%, 0.50 mmol) was added to the mixture followed by addition of solid $NaBH_4$ (0.2 g, 5.29 mmol) in a single act under well stirring condition of the mixture. Then within one minute of the addition of $NaBH_4$, 21 mmol NaOH was added and immediately volume of the solution was made up to 50 ml by water. Other samples E and F were prepared in the similar way as sample D by changing the concentrations of PAA and NaOH. For samples E and F, the amounts of PAA solution taken were 1.6 and 6.4 g, corresponding to 11.38 and 45.53 mmol of PVP (in terms of monomeric units), respectively. For samples E and F the amounts of NaOH added were 80 and 336 mmol, respectively. The pH of the samples was found to lie between 11 and 12.

It is important to mention that maintenance of proper pH of the resulting solution is the essential condition for the synthesis of Ni nanoparticles, otherwise Ni will be further converted to Ni^{2+}.[40] It is also of note that neither PVP nor PAA can reduce Ni^{2+} to Ni at room temperature, so the addition of stronger reducing agent like $NaBH_4$ is required. In our case of synthesis the amounts (in mmol) of NaOH used for the samples were determined by trial and

error experiments. Polymer-Ni nanocomposites were separated by centrifugation. All the experiments were carried out at 30 ± 2˚C.

Characterization of samples

Powder X-ray diffraction (XRD) study of the nickel nano-composites were made with a Rigaku Miniflex diffractometer employing Cu*k*α radiation (λ = 1.541Å) at 30 kV and 15 mA. The 2θ angular region between 30^o and 90^o was explored at a scan rate of 1.000^o/min in a continuous scan mode. The specimens for this study were prepared by adsorbing polymer-nickel nanocomposite (collected by centrifugation) on the fine activated charcoal followed by drying in a vacuum desiccator.

Fourier transform infrared (FTIR) spectroscopy was carried out in Perkin Elmer Spectrum BX2 FTIR Spectroscope. For the measurements, dry solid polymer-metal nanocomposites and neat polymers were used.

The shape and size of the nanoparticles were investigated using high resolution transmission electron microscope (HRTEM) (JEM – 2100 HRTEM, JEOL, Japan) operated at 200 kV. The samples for this study were prepared by sonicating the diluted Ni sols for 5 min and then placing a drop of the mixture onto a 300 mesh carbon-coated copper grid, followed by the natural evaporation of the solvent at room temperature. Measurements from printed enlarged TEM micrographs involved for particles with approximately elliptical profiles, estimates of the equivalent-area circle diameters from long and short-axis measurements. Particle size distributions of the samples were obtained on the basis of measurements form about 300 particles from different micrographs.

Nickel electrodes for electrochemical studies were prepared by typical drop casting technique of chemical solution deposition on graphite (C) substrate. Chemical deposition was made on bare portion of one end of each Teflon enwrapped spectroscopic grade graphite rod (Graphite India Ltd.) of which another end was used for electrical contact. The bare portion

of the graphite rod where the chemical deposition was made has the geometric surface area of ca. 0.24 cm^2. One drop amounting 20 µL of each sample from micropipette was cast onto the bare portion of the graphite rod at one end. Then 10 µL 0.5 % Nafion solution in water was added to fix the catalyst on the graphite rod and dried in vacuum desiccator for over night. Cyclic voltammetric study of these carbon/ nickel electrodes was conducted in a two compartment glass-cell suitable for a conventional three electrode assembly at the scan rate of 0.05 Vs^{-1}, using computer aided Potentiostat/Galvanostat of Autolab PG STAT 12 (Eco chemic, Netherlands). In this study, the reference electrode used was $Hg/HgO/OH^-$(1M) (MMO) having equilibrium electrode potential ~ 0.1 V with respect to standard hydrogen electrode (SHE). A large Pt foil (1 cm × 1 cm) was used as counter electrode and the potentials were measured with respect to MMO.

It should be noted that in order to determine the amounts of metal and polymer in the drops, control experiments have been performed. In short, thirty drops of each sample was collected in watch glass followed by drying in vacuum desiccator for hours to get constant mass of the Ni-polymer nanocomposite. Mettler electronic balance AE 240 was used in the latter case. On the other hand, amount of nickel in each drop of the sample was determined from the atomic absorption spectroscopic (AAS) study. This shows that nickel and polymer mass-ratios in the drops belong virtually to the same as their initial ratio in the respective sample.

Results and discussion

After the addition of $NaBH_4$, all the solutions rapidly turned black irrespective of the used polymers and their concentrations as the Ni^{2+} ions are reduced by borohydride. The stoichiometric equation for the reduction of Ni^{2+} ions can be expressed as[41]:

$$2Ni^{2+} + BH_4^- + 2H_2O = 2Ni^0 + BO_2^- + 2H_2 + 4H^+$$

All the samples (bearing pH: 11 to 12) are found to be highly stable with no color change with time. The stable black color in all the samples clearly suggests the formation of stable dispersions as also suggested by the others.[42]

The crystalline nature of the synthesized nickel nanoparticles of samples A–F were confirmed by X-ray diffraction (XRD) study. Both the representative diffractograms in the Fig. 1 exhibit the same characteristic peaks of crystalline bulk metallic nickel. For both the samples (A and D) three characteristic peaks for nickel (2θ = 44.5°, 51.8° and 76.4°), corresponding to Miller indices (111), (200) and (222) respectively were observed. Thus Fig. 1 shows the XRD pattern of the samples, which are in good agreement with cubic phase nickel, with respect to peak position. The diffraction peaks show a trend of broadening, which results from the reduced size of the particles. Although it is known that nickel is easily oxidized to oxides or hydroxides by water, some possible oxides or hydroxides such as NiO, Ni_2O_3, and $Ni(OH)_2$ were not observed in this study. This might be due to the fact that after the addition of $NaBH_4$, appropriate pH was maintained within the stipulated period of time. Notably, no peak for $NiCl_2$ was found in the diffractograms. This confirms the fact that all the Ni^{2+} ions have converted into Ni(0) under the experimental condition. These results also reveal that in all cases the resultant particles are pure face centered cubic (fcc) nickel, which are also confirmed in the SAED study along with subsequent TEM study.

Figs. 2(a–c) are the HRTEM images of samples A–C whose size distribution histograms are at the respective insets. The TEM images show that the average diameters of the nanoparticles associated with samples A, B and C were 4.6, 3.1 and 1.2 nm with standard deviations of 0.77, 0.76 and 0.15 nm, respectively. Hence, the average particle size decreases with the increase in concentration of PVP for the samples as expected. The HRTEM images for the samples D–F are represented by Figs. 3(a–c). The size distribution histograms associated with the samples are at the inset. The TEM images show that the average

diameters of the nanoparticles for the samples D, E and F were 6.1, 3.7 and 2.2 nm with standard deviations of 0.75, 0.92 and 0.42 nm, respectively. Hence, for the samples, the average particle size decreases with increase in concentration of PAA as well. It appears form all the TEM micrographs that the particles essentially were very fine, nearly spherical, and fairly mono-disperse. For a better quantitative interpretation of the obtained HRTEM results, the mean particle number ($N_{particles}$) and the global particle surface ($S_{particles}$) have been estimated by the following equations:

$$N_{particles} = \frac{6M[Ni(II)]}{\pi\rho d^3}$$

$$S_{particles} = \frac{6M[Ni(II)]}{\rho d}$$

Where Ni(II) is the initial content, M is the molar mass, ρ is the bulk density (8.91 gcm^{-3}) of nickel and d is the particle diameter obtained from HRTEM analysis. The ratio between the number of monomer unit of polymer and the global particle surface (i.e., $n/S_{particles}$) has been calculated for the samples and summarized in Table 1. It clearly appears from the tabulated data that particle-diameter decreases with the increase in concentration of the polymer and hence for the samples both $N_{particles}$ and $S_{particles}$ increases in the order: A < B < C; D < E < F. On the other hand, the values of $n/S_{particles}$ represent the number of monomer units of polymer per unit global surface area of nanoparticles in solution, which is nothing but the average thickness of coating of nickel-polymer nano-composite on graphite substrate when the electrodes are constructed. These suggest that nanoparticle-surface in the electrodes constructed from sample C and F are more overcoated by the polymer moiety as compared to

those constructed from samples A and D, respectively. Further nanoparticle-surface in sample A is relatively more exposed than that of sample D owing to thin average coating of the nickel-polymer nano-composite. It should be noteworthy that alike other metal nanoparticles, after the addition of $NaBH_4$ to the aqueous polymer mixture, nickel seeds are produced by the reduction of Ni^{2+} ions. These seeds collide with their neighbors and hence agglomerate to form small nanoclusters that further grow into the larger clusters. The presence of polymer stabilizer restricts the growth of the clusters, depending upon their concentration. Moreover the polymers with their functional groups seemingly approach to the Ni surface at all the facets (along all axes and planes) such that spherical nanoparticles result. However TEM analyses show that for nearly same number of monomeric units of the polymers, PVP provides smaller nanoparticles than PAA (vide Table 1). Here also the number of monomer unit of polymer per palladium atom is very high causing a labeling effect with respect to the activity of the functional group of polymer. On the other hand the monomer unit of PVP is sterically more bulky and contains larger hydrophobic moiety than that of PAA and hence the former is seemingly capable to provide more steric holes to protect the in situ-generated small metal clusters more effectively. So, average particle diameter in each PVP solution is slightly smaller than that obtained in the corresponding PAA solution. The represented small area electron diffraction (SAED) patterns of nickel nanoparticles are shown in Figs. 2(d) and 3(d) for samples A and D, respectively. In the each representative diffraction pattern three fringe patterns with plane distance of ca. 2.03, 1.76 and 1.02 Å can be observed. They are likely to be related to the (111), (200) and (222) planes of pure fcc nickel as detected in XRD analysis.

The FTIR spectra of polymer-coated Ni nanoparticles and neat polymer are shown in Fig. 4. Typical PVP bands are detected in all the Ni/PVP samples A–C which confirm the presence of polymer in the final samples (Fig. 4(a)). The band at ca. 1662 cm^{-1} in the spectra of PVP is attributed to the C=O stretching of PVP structure. A more detailed observation of

the spectra of sample A in Fig. 4(a) indicates a red shift of this band when compared to neat PVP. The shift of the band to lower energies should be due to the chemical interaction between PVP molecules and the nickel nanoparticle surface.[32] This result represents a strong evidence that the metal interaction occurs with the C=O groups of the PVP. As the PVP/Ni ratio increases the fraction of the bound carbonyl groups decreases, so that the band frequency of the bound carbonyl groups is seemingly losing intensity.[43] Thus in the spectrum of sample B and C, the band is not discernible as the fraction of the bound carbonyl groups is negligibly small compared to that of free PVP in the PVP-Ni(0) nanocomposites.

Since all the samples ultimately attend the pH ranging from 11 to 12 so, it is reasonable to think that carboxylic acid groups of the samples D–F will be converted to carboxylate anion under the synthetic conditions. So, comparative FTIR spectra of both the polymer-stabilized nickel nanoparticles of different initial PAA to nickel ratio and the neat sodium polyacrylate instead of PAA give the insight to the bonding mode of polymer on the nanocluster surface. The FTIR spectra of neat sodium polyacrylate and polymer stabilized Ni nanoparticles in Fig. 4(b) show no essential difference with the exception of the carboxylic acid group region for sample D. In the spectrum of sodium polyacrylate (vide Fig. 4(b)), the band at ca. 1460 cm^{-1} is assigned to the stretching mode of the carboxylate anion. The shift of this band towards lower frequency (at ca. 1408 cm^{-1}) and disappearance of C–H band (observed at 2956 cm^{-1} for PAA or polyacrylate) indicate the interaction of the COO^- groups and the C–H moiety of the polymer with the surface of Ni nanoparticles in sample D. Further, the peak at ca. 700 cm^{-1}in pure polyacrylate, identified as CH_2-rocking vibration is absent in sample D. The disappearance of the peak is seemingly due to well blending behavior of polymer chain with the nanometal.[44] As the PAA/Ni ratio increases the fraction of the bound COO^- groups or C–H moieties decreases, so that the aforesaid frequencies are probably losing intensity. So, in the spectrum of samples E and F, the bands are not perceptible as the

fraction of bound COO^- groups or interacting C–H moieties is negligibly small compared to that of free polymer in the polymer-metal nanocomposites.

Electrocatalytic activity of graphite-supported nickel nanoparticles was examined by cyclic voltammetric study. Before chemical deposition cyclic voltammetric behaviour of graphite (C) substrate was examined. The cyclic voltammetric behavior of this electrode (Fig. 5(a)) in 1M NaOH in presence and absence of 1M MeOH showed insignificant amount of current density for methanol oxidation indicating that methanol is virtually electro-inactive on graphite electrode.[45]

Different cyclic voltammograms (CVs) of the electrodes correspond to the chemically deposited nickel electrodes, C/Ni(1–6) which were constructed from samples A–F respectively. It is of note that under experimental condition all the Ni^{2+} ions are likely to be converted to Ni^0 and all the electrodes possess almost same catalyst (Ni^0) loading as evident from XRD and AAS studies, respectively. Also, it appears from the control experiments that polymer to metal mass-ratio in electrode C/Ni(1) (or C/Ni(4)) is lower than that of C/Ni(3) (or C/Ni(6)). For electrode C/Ni(2) (or C/Ni(5)), this mass-ratio is intermediate between these two. It is well known[45–47] and also shown by our cyclic voltammetric study[48] that oxidation of Ni to $Ni(OH)_2$ in 1M NaOH produces a peak at about -0.5 V and occurs just after hydrogen evolution reaction on Ni at ca. -0.8 V. So, in the present study, Ni nanoparticle surface is expected to be chiefly covered by $Ni(OH)_2$ at the start potential -0.1 V of the potential scan. In the inset CVs of Figs. 5(b) and (c) a peak at ~ 0.47 V in anodic and another one at ~ 0.37 V in cathodic directions, respectively are observed for C/Ni(1 and 4) electrodes for 1M NaOH solution. The couple of peaks corresponds to the redox reaction of $Ni(OH)_2$ to NiOOH and vis-versa in accordance with the eqn (1)[45]:

$$Ni(OH)_2 + OH^- \Longleftrightarrow NiOOH + H_2O + e \qquad (1)$$

In Figs. 5(b) and (c), the profiles for C/Ni(1 and 4) in 1M NaOH (at zone 2) show peaks at ~ 1.04 V (forward scan) and ~ 0.97 V (backward scan). This is seemingly due to formation of higher valence nickel e.g. Ni^{4+} [49] and its conversion to NiOOH which can be expressed as follows:

$$NiOOH + OH^- \Longleftrightarrow NiO_2 + H_2O + e \quad (2)$$

This is supported by E^0 values of $NiO_2/Ni(OH)_2$ (0.76 V) and $NiOOH/Ni(OH)_2$ (0.43 V) as found in the literature.[50] These values are used to compute E^0 of reaction (2) which is -1.09 V indicating greater difficulty of formation of Ni^{4+} from Ni^{3+}. Reportedly, electrochemical oxidation of methanol at nickel electrodes can be presented by[51, 52]:

$$Ni(OH)_2 \rightarrow NiOOH + H^+ + e \quad (3)$$

$$NiOOH + \text{methanol} \rightarrow Ni(OH)_2 + \text{Oxidation products of methanol} \quad (4)$$

The active NiOOH formed during the positive potential scan is consumed through reaction (4). Subsequently, the $Ni(OH)_2$ formed in reaction (4) is again oxidized to NiOOH during the anodic potential sweep. Thus the otherwise reversible[45, 48] reverse cathodic peak of NiOOH at ~ 0.37 V disappears during methanol oxidation.

The profiles (Figs. 5(b) and (c)) for C/Ni(1 and 4) in alkaline (1M) MeOH (1M) show two peaks at ~ 0.71 and ~ 0.68 V (zone 1) and other two peaks at ~ 1.10 and ~ 0.94 V (zone 2) in positive potential or forward scan direction. In zone 1 the peak for forward scan corresponds to oxidation of MeOH by NiOOH [45, 52] and the peak (zone 2) for forward scan seemingly corresponds to oxidation of MeOH at higher valence nickel e.g. Ni^{4+} [49] respectively. It is also noteworthy that Van Effan and Evans [45] found that the oxidation of ethanol in KOH solution involved the catalysis of higher valence nickel oxide, which acts as chemical oxidizing agent.

Figs. 5(d) and (e) represent the CVs of C/Ni(1–3) and C/Ni(4–6) electrodes in alkaline methanol, respectively with respective CVs of the electrodes in 1M NaOH (inset). The peak

current density (i_F and i_B) and corresponding potentials (E_F and E_B) are summarized in Table2. The table reveals that the peak potential values are lower with nanoparticles of smaller diameters for each Ni-polymer electrode system indicating better intrinsic catalytic activity for smaller nanoparticles. The peak currents of C/Ni(1–6) electrodes at zone 1 follow the order:

C/Ni(2) > C/Ni(1) > C/Ni(3);

C/Ni(4) > C/Ni(5) > C/Ni(6).

These orders are not expected on the basis of particle size alone associated with the electrodes. Particle size effect competes over the thickness of the polymer coating in the first case where polymer coating is thin. In other cases, MeOH penetrates the thicker polymer layer of the particles with more difficulty in the potential region studied as evident from the peak current density (vide Table 2). For C/Ni(4) electrode where polymer coating is thin the effect of particle-surface-environment dominates over the effect of particle size because negatively charged polyacrylate interacts more with the nanoprticles at positive potentials. Thus bigger nanoparticles bearing low relative amounts of polymer provide higher peak current density values. So in most cases it seems reasonable to suggest that the hindrance/ surface coverage by the adsorbed capping polymer presumably overcome the size effect. This is consistent with the observation that the relative amounts of the polymer adsorbed per unit surface of metal nanoparticles (see Table 1). This is also in conformation with similar observations that adsorption of polymer on the particle-surface and that in the solution are important for the catalytic application as adsorption of the polymer can decrease the activity of the particles.[53]

On the other hand, in zone 2 for C/Ni(1–3) electrodes the order of current density values is C/Ni(3) > C/Ni(2) > C/Ni(1) indicating smaller nickel nanoparticles provide greater current density presumably because the in-situ generated NiO_2 specis are not well capped by

the polymer. On the contrary the order is reversed for C/Ni(4–6) electrodes i.e., C/Ni(4) > C/Ni(5) > C/Ni(6). Both these orders are the same for the peak current density of the electrodes in 1M NaOH (vide the insets of Figs. 5(d) and (e)). This can be explained by considering the fact that at the surface of smaller nanoparticles, formation of higher valence nickel species (e.g. Ni^{4+}) is favored for C/Ni(1–3) electrodes, as expected on the basis of particle size. But the situation is reverse for C/Ni(4–6) electrodes. In the latter case, stronger binding of increasingly positive charged nanoparticle surface with the polymer's functional group (carboxylate anion) for smaller nanoparticles, probably restrict methanol molecules to approach to the metal surface for reaction. So, the difference in electrocatalytic activity for the electrodes results from the difference in embedded nanoparticle size, thickness of the polymeric encapsulation on particle surface, nature of particle-polymer interaction, and otherwise. It may be concluded that the effect of particle-surface-environment competes with that of particle size of polymer-stabilized nickel nanoparticles in dictating the electrocatalytic activity for methanol oxidation. Further PVP protects the nanoparticles by its bulky pyrrolidone moiety whereas polyacrylate protects the same by its negatively charged carboxylate groups at positive potentials.

Moreover, it is interesting to state that the dependence of the current density of anodic peak has a good linear dependence on MeOH concentration in the concentration region shown in Fig. 6 indicating that the material can be considered as a sensor for MeOH and can be used for the measurement of MeOH concentration. However, it is remarkable that in zone 1 current density increases with the concentration of MeOH in all cases, as expected but in zone 2 current density for C/Ni(6) electrode decreases with the concentration of MeOH. The reverse trend of latter may be due to the fact that when the MeOH concentration is high, in the electrode surface wings, the intermediates resulting from MeOH oxidation was not oxidized completely and its concentration is so high, that it blocks the surface. Usually the

M-CO like intermediate is consumed by the adjacent adsorbed M-OH (M=Ni).[54] But here such reaction is not possible owing to the hindrance of the acrylate anion near the more positive surface of the metal at the high potential. Consequently, surface blocking by the unconsumed intermediate species seemingly causes decrease of current density in zone 2 of electrode C/Ni(6).

Conclusions

Polymer-protected stable nickel nanoparticles (1.2–6.1 nm) have been synthesized by the sodium borohydride reduction of nickel chloride in aqueous solution by separately using two polymers e.g., PVP and PAA as stabilizer. It was found that maintenance of pH was essential in order to synthesize stable nickel nanoparticles. In this synthesis samples with different nickel/polymer ratios were obtained and average particle diameters were found to decrease when the ratio Ni(II)/polymer was decreased. TEM study clearly shows that the as-synthesized Ni nanoparticles are fairly monodisperse and are in the nano-size domain. For nearly same number of monomeric units of the polymers, PVP leads to the formation of smaller nanoparticles than that furnished by PAA as determined by TEM study. The resultant particles have been characterized to be pure crystalline nickel of fcc structure by XRD and also SAED studies. In the polymer-metal nanocomposites, polymer was found to co-ordinate with the nanoparticle surface through some of the functional groups as concluded from comparative FTIR spectroscopic study. In alkaline medium at higher potentials, the synthesized nickel nanoparticles form $Ni(OH)_2$ and then NiOOH followed by higher valence Ni species. The in situ generated $Ni(OH)_2$ and NiOOH are electrocatalytically active towards the alkaline oxidation of methanol and act as a sensor-material for methanol as determined by cyclic voltammetry. These active nanoparticles exhibit competing effects in size- and particle-surface-environment in electrocatalytic activity as shown in cyclic voltammetric

study. For PAA-stabilized nanoparticles effect of particle-surface-environment predominates over the particle size effect in dictating the peak current values. On the other hand, for electrodes comprised of PVP-stabilized nanoparticles, the effect of particle size and particle-surface-environment overcome one another in guiding the peak current density depending on the potential.

References

1 Y. Gao, J. Zhao, B. Zhou, Y. Zhu, Z. Wang, *Colloids and Surf. A: Physicochem. Eng. Asp.* , 2010, **368**, 137.

2 M. Wen, Y. F. Wang, F. Zhang, Q. S. Wu, *J. Phys. Chem. C*, 2009, **113***,* 5960.

3 D. Astruc, F. Lu and J. R. Aranzaes, Angew. Chem., Int. Ed., 2005, **44**, 7852.

4 G. G. Couto, J. J. Klein, W. H. Schreiner, D. H. Mosca, A. J.A. de Oliveira, A. J. G. Zarbin, J. Colloid Interface Sci., 311 (2007) 461.

5 H. T. Zhang, J. Ding, G. M. Chow, M. Ran, J. B. Yi, *Chem. Mater.*, 2009, **21**, 5222.

6 Y. Chen, D. -L. Peng, D. Lin and X. Luo, *Nanotechnology*, 2007, **18**, 505703.

7 Z. Zhu, X. Guo, S. Wu, R. Zhang, J. Wang and L. Li, *Ind. Eng. Chem. Res.* 2011, **50**, 13848.

8 S. M. A. Shibli, K. S. Beenakumari and N. D. Suma, Biosens. Bioelectron., 2006, **22**, 633.

9 N. M. Suleimanov, S. M. Khantimerov, E. F. Kukovitsky and V. L. Matukhin, J. Solid State Electrochem., 2008, **12**, 1021.

10 J. Bagchi and S. K. Bhattacharya, Transition Met. Chem., 2008, **33**, 113.

11 Z. G. Wu, M. Munoz, O. Montero, *Adv. Powder Technol.*, 2010, **21***,* 165.

12 X. Yue, H. Fu, D. Li, *Appl. Mechanics Mater.,* 2011, **80**, 217.

13 L. Li and L. Dai, Nanotechnology, 2005, **16,** 2111.

14 D. de. Caro, J. S. Bradley, *Langmuir*, 1997, **13**, 3067.

15 P. Singjai, K. Wongwigkarn, Y. Laosiritaworn, R. Yimnirun, S. Maensiri, Current Appl. Phys., 2007, **7**, 662.

16 J. H. Choi, T. Y. Lee, S. H. Choi, J.-H. Han, J.-B. Yoo, C.-Y. Park, T. Jung, S. G. Yu, W. Yi, I.-T. Han, J. M. Kim, Diamond and Related Mater., 2003, **12**, 794.

17 Z. Wu, S. Ge, M. Zhang, W. Li, K. Tao, *J. Colloid Interface Sci.*, 2009, **330**, 359.

18 J. Zhang, C. Q. Lan, *Mater. Lett.*, 2008, **62**, 1521.

19 K. Y. Jung, J. H. Lee, H. Y. Koo, Y. C. Kang, S. B. Park, *Mater. Sci. Eng. B*, 2007, **137**, 10.

20 W. Xu, K. Y. Liew, H. Liu, T. Huang, C. Sun, Y. Zhao, *Mater. Lett.* 2008, **62**, 2571.

21 Y. Hou, S. Gao, *J. Mater. Chem.*, 2003, **13**, 1510.

22 M. Green and P. O'. Brien, *Chem. Commun.*, 2001, **1912**.

23 D. -H. Chen and C. -H. Hsieh, *J. Mater. Chem.,* 2002, **12**, 2412.

24 L. Chen, J. Chen, H. Zhou, D. Zhang and H. Wan, *Mater. Sci. Eng. A*, 2007, ***452/453***, 262.

25 Y. T. Jeon, J. Y. Moon, G. H. Lee, J. Park and Y. Chang, *J. Phys. Chem. B*, 2006, **110**, 1187.

26 Y. Jeon, G. H. Lee, J. Park, B. Kim and Y. Chang, *J. Phys. Chem. B*, 2005, **109**, 12257.

27 T. Hinotsu, B. Jeyadevan, N. C. Chinnasamy, K. Shinoda and K. Tohji, *J. Appl. Phys.,* 2004, **95**, 7477.

28 N. C. Chinnasamy, B. Jeyadevan, K. Shinoda, K. Tohji, A. Narayanasamy, K. Sato and S. Hisano, *J. Appl. Phys.*, 2005, **97**, 10J309.

29 V. Tzitzios, G. Basina, M. Gjoka, V. Alexandrakis, V. Georgakilas, D. Niarchos, N. Bonkos and D. Petridis, *Nanotechnology*, 2006, **17**, 3750.

30 T. Umegaki, J. -M. Yan, X. -B. Zhang, H. Shioyama, N. Kuriyama, Q. Xu, *Int. J. Hydrogen Energy*, 2009, **34**, 3816.

31 Y. -L. Hou, S. Gao, *J. Alloys Compd.*, 2004, **365**, 112.

32 G. G. Couto, J. J. Klein, W. H. Schreiner, D. H. Mosca, A. J. A. de Oliveira, A. J. G. Zarbin, *J. Colloid Interface Sci.*, 2007, **311**, 461.

33 J. W. Yoo; S. -M. Lee; H. -T. Kim and M. A. El-Sayed, *Bull. Korean Chem. Soc.*, 2004, **25(3)**, 395.

34 Z. Konya, V. F. Puntes, I. Kiricsi, J. Zhu, P. Alivisatos and G.A. Somorjai, *Catal. Lett.*, 2002, **81(3–4)**, 137.

35 B. Yoon, H. Kim and C. M. Wai, *Chem. Commun.*, 2003, **1040**.

36 P. S. Roy, J. Bagchi, S. K. Bhattacharya, *Trans. Met. Chem.*, 2009, **34**, 447.

37 P. S. Roy, J. Bagchi, S. K. Bhattacharya, *Colloids Surf. A: Physicochem. Eng. Asp.*, 2010, **359**, 45.

38 P. S. Roy, J. Bagchi, S. K. Bhattacharya, *Catal. Sci. Technol.*, 2012, **2**, 2302.

39 P. S. Roy, S. K. Bhattacharya, *Catal. Sci. Technol.*, DOI: 10.1039/c3cy20686f.

40 X. Xu, Y. Yin, X. Ge, H. Wu, Z. Zhang, *Mater. Lett.*, 1998, **37**, 354.

41 H. Zhu, Y. Jia, X. Wu, H. Wang, *J. Hazardous materials*, 2009, **172**, 1591.

42 D. S. Sidhaye, T. Bala, S. Srinath, H. Srikanth, P. Poddar, M. Sastry and B.L.V. Prasad, *J. Phys. Chem. C*, 2009, **113(9)**, 3426.

43 Ö. Metin, S. Özkar, *J. Mol. Catal. A: Chem.*, 2008, **295**, 39.

44 N. Giri, R. K. Natarajan, S. Gunasekaran and S. Shreemathi, *World J. Sci. Technol.* 2011, **1(7)**, 54.

45 M. A. Abdel Rahim, R. M. Abdel Hameed, M. W. Khalil, *J. Power Sources*, 2004, **134**, 160.

46 A. Seghiouer, J. Chevalet, A. Barhoun, F. Lantelme, *J. Electroanal. Chem.*, 1998, **442**, 113.

47 M. Vukovic, J. Appl. *Electrochem.*, 1994, **24**, 878.

48 J. Bagchi, S. K. Bhattacharya, *Trans. Metal Chem.*, 2007, **32**, 47.

49 E. Gileadi, E. Kirowa-Eisner, J. Penciner, *Interfacial Electrochemistry*, Addison-Wesley Publishing Company, Inc., Massachusetts, USA, 1975.

50 R. C. Weast and G. L. Tuve (Eds.), *Handbook of Chemistry and Physics*, CRC Press, 52nd Edition, 1971–1972.

51 A. N. Golikand, S. Shahrokhian, M. Asgari, M. G. Maragheh, L. Irannejad; A. Khanchi, *J. Power Sources*, 2005, **144**, 21.

52 M. G. Hosseini, M. M. Momeni, M. Faraji, *Electroanalysis*, 2010, **22(22)**, 2620.

53 A. Pal, S. Shah, S. Belochapkine, D. Tanner, E. Magner, S. Devi, *Colloids Surf. A: Physicochem. Eng. Asp.*, 2009, **337**, 205.

54 C. Bianchini, P. K. Shen, *Chem. Rev.*, 2009, **109(9)**, 4183.

Acknowledgments

We the authors gratefully acknowledge Jadavpur University for financial assistance.

Figure Captions

Fig. 1 Representative X-ray diffractograms of charcoal adsorbed Ni-nanoparticles from samples A and D.

Fig. 2 TEM micrographs (a–c) of polymer-protected Ni nanoparticles from samples A–C; in Fig. 2(a) nanoparticles are a few in numbers and not found everywhere of the image are marked by the loops; inset of Fig. 2(a): Typical magnified view from sample A. Frequency (%) versus Diameter (nm) plot of nanoparticles in the histogram is shown in the inset of the corresponding TEM image. (d) Representative diffraction pattern of the Ni nanoparticles from sample A.

Fig. 3 TEM micrographs (a–c) of polymer-protected Ni nanoparticles from samples D–F; inset of Fig. 3(c): Typical magnified view from sample C. Frequency (%) versus Diameter (nm) plot of nanoparticles in the histogram is shown in the inset of the corresponding TEM image. (d) Representative diffraction pattern of the Ni nanoparticles from sample D.

Fig. 4(a) FTIR spectra of polymer-Ni nanocomposites corresponding to samples A–C and the neat polymer.

Fig. 4(b) FTIR spectra of polymer-Ni nanocomposites corresponding to samples D–F and the neat polymer.

Fig. 5 (a) CVs of charcoal (C) in NaOH (1M) in presence and absence of MeOH (1M).

Fig. 5 CVs of C/Ni(1) electrode (b) and that of C/Ni(4) electrode (c) in NaOH (1M) in presence and absence of MeOH (1M). The each inset represents the magnified view of the encircled portion of Zone 1 (restricted to 0.3 to 0.6 V) of respective profiles.

Fig. 5 CVs of the C/Ni(1–3) (d) and C/Ni(4–6) (e) electrodes in alkaline (1M) methanol (1M). Each inset represents the corresponding CV set of the respective electrodes in 1M NaOH, obtained from control experiments.

Fig. 6 Plot of current density against the CH_3OH concentration for the two representative electrodes C/Ni(3) and C/Ni(6), showing linear dependence of current density on concentration. Notably, correlation co-efficients for electrode C/Ni(3) are 0.9994 (zone 1) and 0.9999 (zone 2) and for electrode C/Ni(6) are 0.9989 (zone 1) and -0.9955 (zone 2).

Tables

Table 1 Physical characteristic of polymer-protected Ni nanoparticles in 100 ml sample.

Samples	Particle size/nm	Number of monomer unit of polymer (n) $\times 10^{-20}$	$N_{particles} \times 10^{-15}$	$S_{particles} \times 10^{-18}$	$n \times 10^{-2}/S_{particles}$ (unit/nm^2)
A	4.6 ± 0.77	32.52	129.31	8.592	3.785
B	3.1 ± 0.76	130.1	422.50	12.75	10.20
C	1.2 ± 0.15	520.2	7283.9	32.93	15.80
D	6.1 ± 0.75	34.21	55.452	6.479	5.280
E	3.7 ± 0.92	137.1	248.49	10.68	12.84
F	2.2 ± 0.42	548.4	1182.1	17.96	30.54

Table 2 Characteristics of C/Ni(1–6) electrodes constructed from samples A–F, respectively for the oxidation of alkaline (1M) methanol (1M).

[a]Electrodes	[b]Diameter (nm) of the embedded nanoparticles	[c]Zone 1				[d]Zone 2			
		i_F	E_F	i_B	E_B	i_F	E_F	i_B	E_B
C/Ni(1)	4.6	43.26	0.70	46.15	0.69	76.05	1.10	20.51	0.93
C/Ni(2)	3.1	44.42	0.71	48.47	0.68	80.67	1.10	20.50	0.93
C/Ni(3)	1.2	23.20	0.66	25.52	0.62	88.58	1.05	26.10	0.90
C/Ni(4)	6.1	50.61	0.71	56.74	0.68	106.08	1.11	32.69	0.94
C/Ni(5)	3.7	42.80	0.70	46.08	0.67	81.94	1.10	20.35	0.93
C/Ni(6)	2.2	14.76	0.65	16.45	0.61	62.33	1.05	15.29	0.89

N.B. [a]Ni^0 loading of each electrode is 1.56 ± 0.03 μmolcm^{-2}.

[b]Average particle sizes are in accordance with the TEM study.

[c, d]i_F and i_B of zone 1 and 2 are the peak current density for the forward and backward scan, respectively and expressed in mAcm^{-2}. i_F and i_B values include experimental error within 2%.

[c, d]E_F and E_B of zone 1 and 2 are the peak potentials for the forward and backward scan, respectively and expressed in Volt.

Figures

Fig. 1

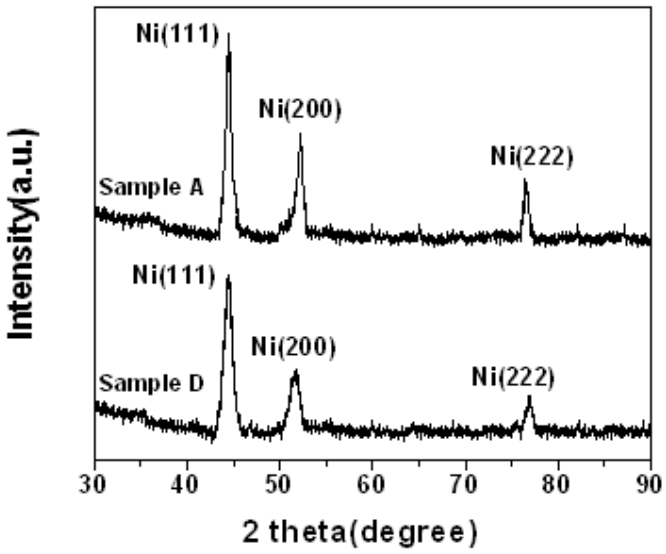

Fig. 1 Representative X-ray diffractograms of charcoal adsorbed Ni-nanoparticles from samples A and D.

Fig. 2

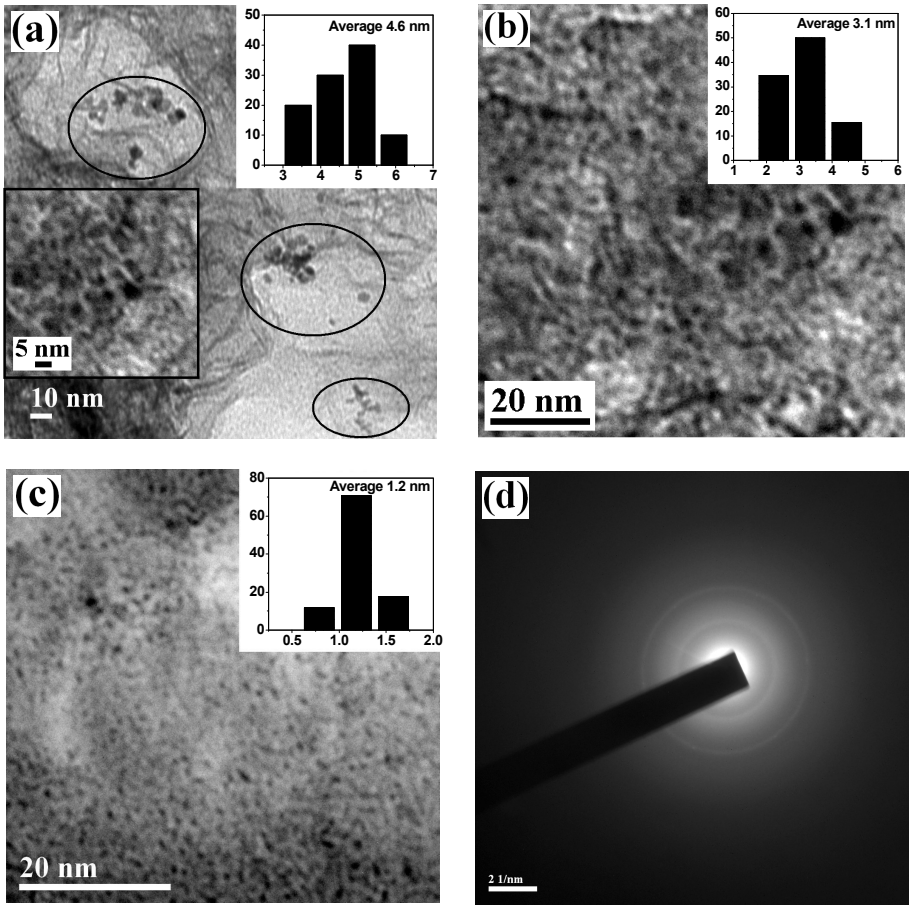

Fig. 2 TEM micrographs (a–c) of polymer-protected Ni nanoparticles from samples A–C; in Fig. 2(a) nanoparticles are a few in numbers and not found everywhere of the image are marked by the loops; inset of Fig. 2(a): Typical magnified view from sample A. Frequency (%) versus Diameter (nm) plot of nanoparticles in the histogram is shown in the inset of the corresponding TEM image. (d) Representative diffraction pattern of the Ni nanoparticles from sample A.

Fig. 3

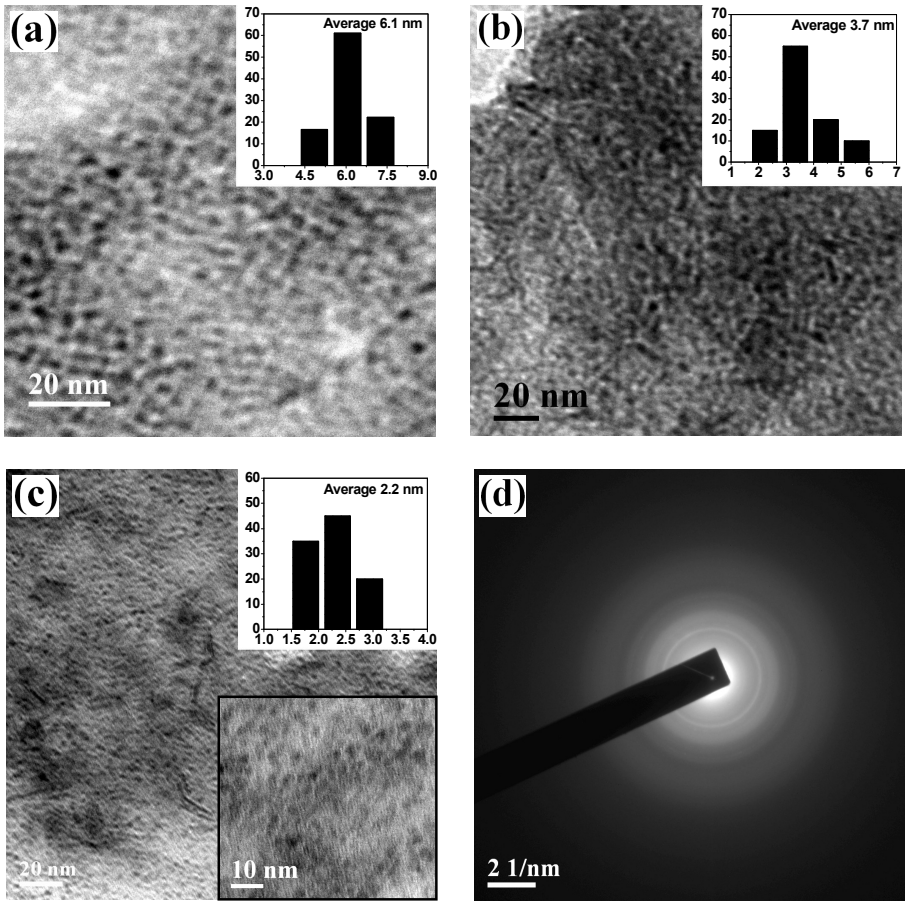

Fig. 3 TEM micrographs (a–c) of polymer-protected Ni nanoparticles from samples D–F; inset of Fig. 3(c): Typical magnified view from sample C. Frequency (%) versus Diameter (nm) plot of nanoparticles in the histogram is shown in the inset of the corresponding TEM image. (d) Representative diffraction pattern of the Ni nanoparticles from sample D.

Fig. 4

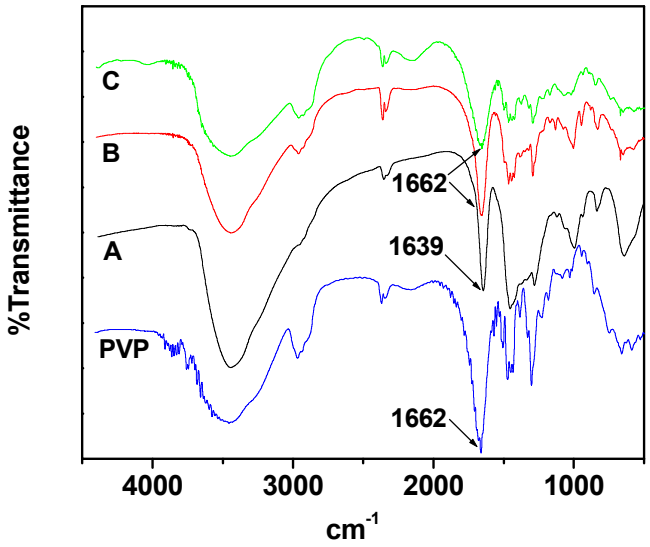

Fig. 4 (a) FTIR spectra of polymer-Ni nanocomposites corresponding to samples A–C and the neat polymer.

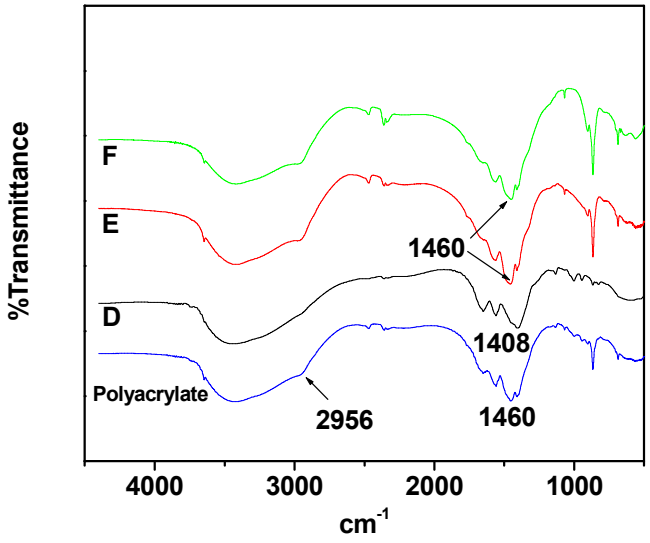

Fig. 4 (b) FTIR spectra of polymer-Ni nanocomposites corresponding to samples D–F and the neat polymer.

Fig. 5

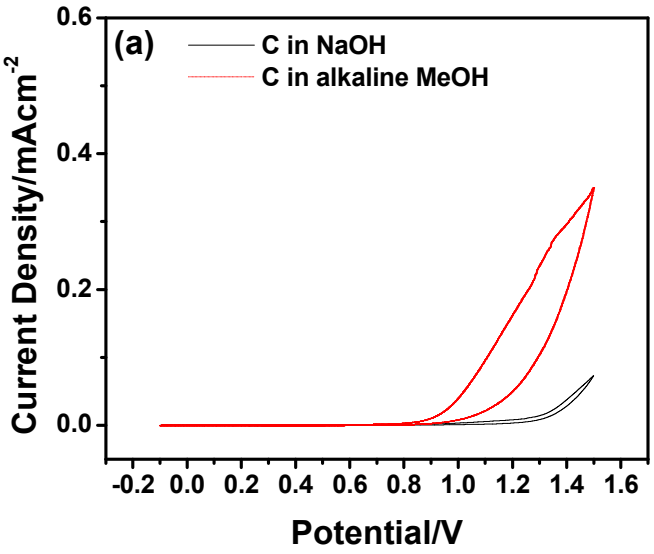

Fig. 5 (a) CVs of charcoal (C) in NaOH (1M) in presence and absence of MeOH (1M).

Fig. 5

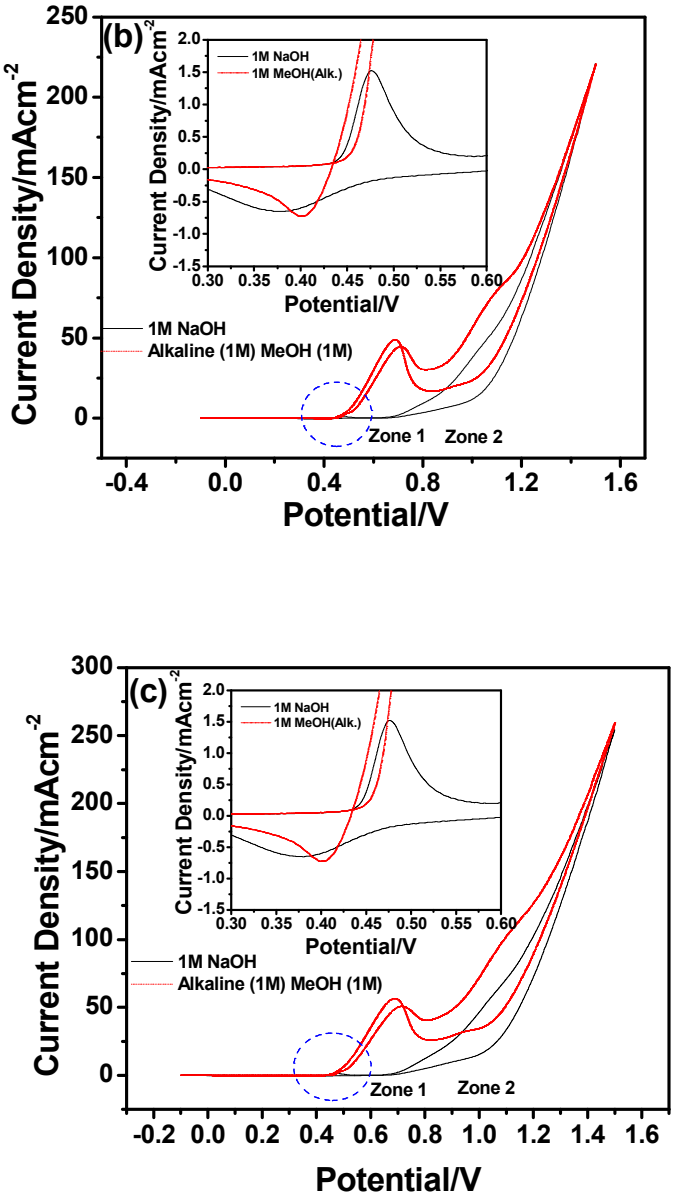

Fig. 5 CVs of C/Ni(1) electrode (b) and that of C/Ni(4) electrode (c) in NaOH (1M) in presence and absence of MeOH (1M). The each inset represents the magnified view of the encircled portion of Zone 1 (restricted to 0.3 to 0.6 V) of respective profiles.

Fig. 5

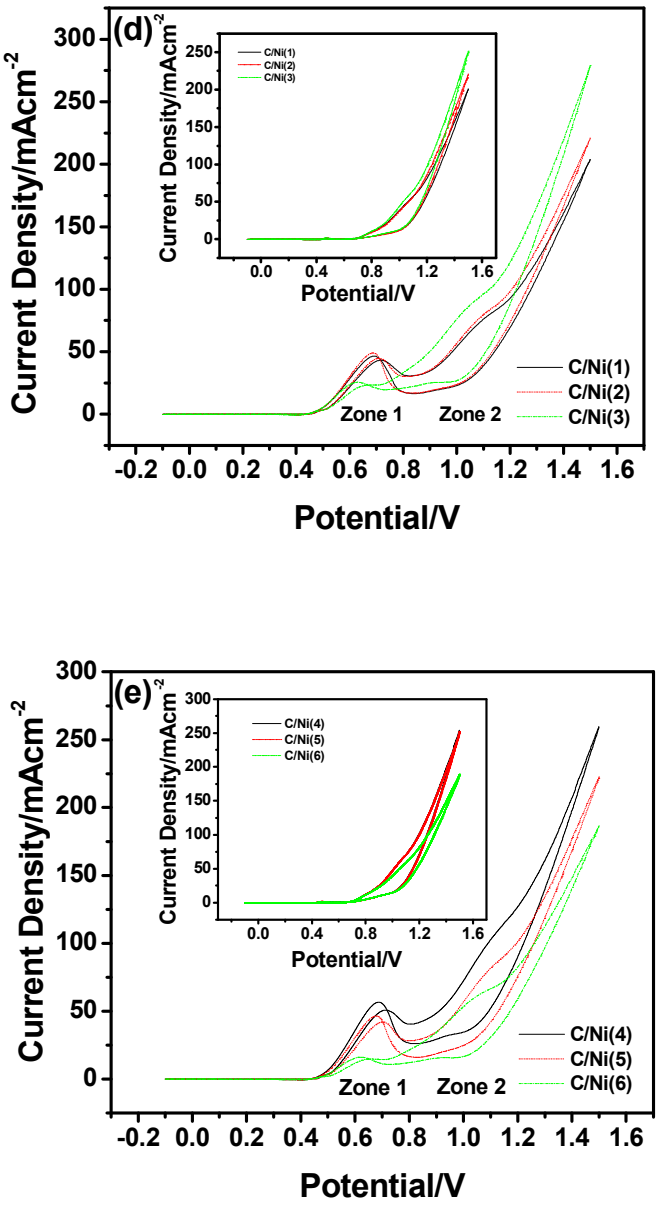

Fig. 5 CVs of the C/Ni(1–3) (d) and C/Ni(4–6) (e) electrodes in alkaline (1M) methanol (1M). Each inset represents the corresponding CV set of the respective electrodes in 1M NaOH, obtained from control experiments.

Fig. 6

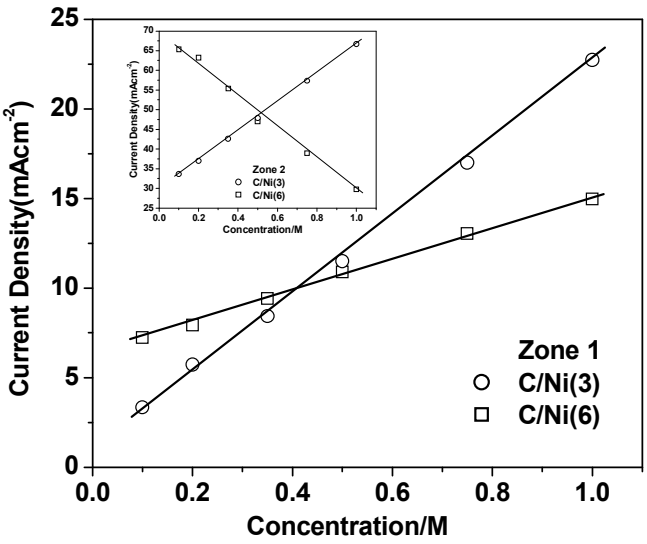

Fig. 6 Plot of current density against the CH_3OH concentration for the two representative electrodes C/Ni(3) and C/Ni(6), showing linear dependence of current density on concentration. Notably, correlation co-efficients for electrode C/Ni(3) are 0.9994 (zone 1) and 0.9999 (zone 2) and for electrode C/Ni(6) are 0.9989 (zone 1) and -0.9955 (zone 2).